Endocrinology, 2021, Vol. 162, No. 1, 1–11
doi:10.1210/endocr/bqaa211
Research Article

Research Article

Glucagon Receptor Inhibition Reduces Hyperammonemia and Lethality in Male Mice with Urea Cycle Disorder

Katie Cavino,[1] Biin Sung,[1] Qi Su,[1] Erqian Na,[1] Jinrang Kim,[1] Xiping Cheng,[1] Jesper Gromada,[1] and Haruka Okamoto[1]

[1]Regeneron Pharmaceuticals, Tarrytown, New York 10591, USA

ORCiD numbers: 0000-0002-6121-9589 (H. Okamoto).

Received: 7 August 2020; Editorial Decision: 10 November 2020; First Published Online: 18 November 2020; Corrected and Typeset: 18 December 2020.

Abstract

The liver plays a critical role in maintaining ammonia homeostasis. Urea cycle defects, liver injury, or failure and glutamine synthetase (GS) deficiency result in hyperammonemia, serious clinical conditions, and lethality. In this study we used a mouse model with a defect in the urea cycle enzyme ornithine transcarbamylase (*Otc*$^{spf\text{-}ash}$) to test the hypothesis that glucagon receptor inhibition using a monoclonal blocking antibody will reduce the hyperammonemia and associated lethality induced by a high-protein diet, which exacerbates disease. We found reduced expression of glutaminase, which degrades glutamine and increased expression of GS in livers of *Otc*$^{spf\text{-}ash}$ mice treated with the glucagon receptor blocking antibody. The gene expression changes favor ammonia consumption and were accompanied by increased circulating glutamine levels and diminished hyperammonemia. *Otc*$^{spf\text{-}ash}$ mice treated with the glucagon receptor-blocking antibody gained lean and body mass and had increased survival. These data suggest that glucagon receptor inhibition using a monoclonal antibody could reduce the risk for hyperammonemia and other clinical manifestations of patients suffering from defects in the urea cycle, liver injury, or failure and GS deficiency.

Key Words: glucagon receptor, hyperammonemia, monoclonal antibody, urea cycle, amino acids, liver

The liver allows for efficient detoxification of ammonia through urea synthesis and condensation of ammonia with glutamate to glutamine. Glutamine serves as a nontoxic interorgan ammonia carrier and as an amino moiety donor for the synthesis of nucleotides, amino acids, amino-sugars, and oxidized nicotinamide alanine dinucleotide. Urea cycle defects, liver injury, or failure and glutamine synthetase (GS) deficiency are linked to hyperammonemia, serious clinical conditions, and in some cases lethality (1–5). The liver is composed of lobules, which are concentric layers of hepatocytes expanding from the central vein toward the periportal vein. The hepatocytes closest to the branches of the portal vein are responsible for the formation of urea, whereas the hepatocytes closest to the central vein express GS. The blood flows from the periportal to the central vein, and the ammonia not used for urea synthesis is taken up

ISSN Online 1945-7170

by the perivenous hepatocytes and converted to glutamine. The compartmentalization of urea formation and glutamine synthesis allows for efficient control of whole-body ammonia levels and prevents spillover of hepatic ammonia into the circulation (6–8).

The urea cycle detoxifies excess ammonia via the sequential reactions of 6 enzymes. The liver is the only organ with a complete set of the enzymes. Deficiency in 1 or more of the enzymes causes urea cycle disorder, characterized by episodes of acute metabolic decompensation with hyperammonemia. The severity depends on the gene as well as the position of the mutation in the gene. Ornithine transcarbamylase (OTC) deficiency is the most prevalent form characterized by recurrent and life-threatening episodes of hyperammonemia (9–11). Urea cycle disorders can be diagnosed at any age. However, the more severe forms occur in the neonatal period and are associated with up to 50% mortality (12–14). Affected infants who survive the neonatal period are chronically at risk for repeated bouts of hyperammonemia and often undergo liver transplantation. Alternative treatment options include dietary protein restriction and nitrogen disposal using phenylbutyrate directing nitrogen for kidney excretion (15–17). Given the lack of effective therapeutic options, there is a need to develop therapies to treat the conditions and prevent hyperammonemia.

Glucagon controls plasma amino acid levels via regulation of hepatic amino acid turnover. This is supported by findings that administration of glucagon to animals and humans results in reductions in plasma amino acids, increased amino acid uptake by the liver, and their conversion into gluconeogenic precursors promoting hepatic glucose production (18, 19). Conversely, genetic or pharmacological inhibition of hepatic glucagon signaling reduces hepatic amino acid turnover, resulting in elevated plasma amino acid levels (20–25). Of importance for this study is that hepatic expression of glutaminase, catalyzing the conversion of glutamine to ammonia and glutamate, is reduced following inhibition of glucagon signaling (26). Moreover, glucagon receptor (GCGR) inhibition in mice using a monoclonal blocking antibody elevates plasma glutamine levels by 4-fold (22). Thus, GCGR signaling blockade may direct excess nitrogen to glutamine, and reduce hepatic ammonia production and spill over to the circulation.

To test the hypothesis that GCGR inhibition will reduce hyperammonemia we turned to $Otc^{spf\text{-}ash}$ mice, a widely used model of urea cycle disorder. $Otc^{spf\text{-}ash}$ mice carry a point mutation in the last nucleotide of exon 4 of the *Otc* gene, which affects 5' splicing and causes 95% reduction in OTC enzymatic activity (27). $Otc^{spf\text{-}ash}$ mice exhibit plasma ammonia levels in the normal range on regular chow diet, but rapidly develop hyperammonemia on a high-protein diet (28). In this study, we assessed the impact of GCGR inhibition on clinical manifestations associated with OTC deficiency by a high-protein diet-induction of hyperammonemia in $Otc^{spf\text{-}ash}$ mice, followed by chronic administration of a GCGR blocking antibody.

Materials and Methods

In vivo studies

The characteristics of the monoclonal GCGR blocking antibody REGN1193 have been reported previously (23, 29). The GCGR antibody and hIgG4 isotype control antibody (30) were diluted with sterile phosphate-buffered saline (PBS). Male $Otc^{spf\text{-}ash}$ mice (The Jackson Laboratory Stock No. 001811) and corresponding wild-type male mice (The Jackson Laboratory Stock No. 001875) were housed 1 to 5 mice per cage in a controlled environment (12-hour light/dark cycle, 22 ± 1°C, 60–70% humidity) and fed ad libitum with regular chow (PicoLab Rodent Diet 20 EXT IRR 5R53; LabDiet; St. Louis, MO, USA) until study initiation. Two-month-old $Otc^{spf\text{-}ash}$ mice (n = 20) and wild-type mice (n = 20) were placed on a 30% protein diet (LabDiet 5001 with 30% Protein; TestDiet; St. Louis, MO, USA) on day 0 and remained on the diet for the duration of the study. $Otc^{spf\text{-}ash}$ and wild-type mice were each sorted into 2 groups based on their plasma ammonia levels on day 2. From day 2 to the end of the study, half of the $Otc^{spf\text{-}ash}$ (n = 10) and wild-type (n = 10) mice received weekly subcutaneous injections of GCGR antibody at 10 mg/kg, whereas the other half of $Otc^{spf\text{-}ash}$ (n = 10) and wild-type (n = 10) mice received weekly subcutaneous injections of the control antibody at 10 mg/kg. Plasma was collected at baseline, day 2, and thereafter every 5 to 12 days to determine ammonia levels. Body weights and nonfasting blood glucose were measured weekly. Blood and plasma were collected at the ad libitum fed condition, with a consistent collection of blood at 9:00 AM and plasma between 10:00 AM and 12:00 PM. Deaths of animals were recorded daily. For the survival study (Fig. 1A–1C), mice were taken down on day 85 without tissue collection. Two duplicate treatment studies were conducted in $Otc^{spf\text{-}ash}$ and wild-type mice using 20 mice per group. One study focused on plasma amino acid quantification on day 21, plasma glucagon measurements on day 37, and liver and pancreas collection on day 41, whereas in the other study liver, kidney, heart, epididymal fat, and skeletal muscle were collected on day 56. All experiments were performed in accordance with the Assessment and Accreditation of Laboratory Animal Care International and in compliance with protocols approved by the Regeneron Pharmaceuticals Institutional Animal Care and Use Committee.

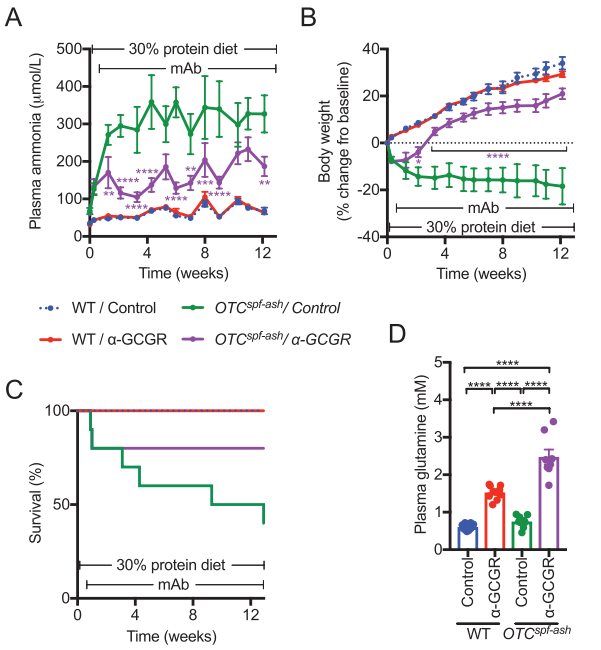

Figure 1. Glucagon receptor (GCGR)-blocking antibody reduces hyperammonemia and mortality in high-protein diet fed *Otc*$^{spf\text{-}ash}$ mice. Plasma ammonia levels (**A**) in *Otc*$^{spf\text{-}ash}$ and wild-type (WT) mice placed on a high-protein diet on day 0 and administered weekly with α-GCGR or control antibodies for 83 days from day 2 (10 mg/kg; n = 10 per group at the study initiation). WT/control antibody (blue); WT/α-GCGR antibody (red); *Otc*$^{spf\text{-}ash}$ mice/control antibody (green); *Otc*$^{spf\text{-}ash}$ mice/α-GCGR antibody (purple). Body weights (**B**), survival curves (**C**), and day 21 plasma glutamine levels (**D**) in the treatment groups described in (**A**). Data are mean ± standard error of the mean (SEM). Statistical analysis was conducted by 2-way (**A**, **B**) or 1-way (**D**) analysis of variance (ANOVA) with Bonferroni post-test. Comparisons were made between the *Otc*$^{spf\text{-}ash}$/α-GCGR group and the *Otc*$^{spf\text{-}ash}$/control group (**A**, **B**). * $P < 0.05$, ** $P < 0.01$, *** $P < 0.001$, **** $P < 0.0001$.

Blood chemistry

Plasma ammonia was assayed in a Siemens ADVIA Chemistry XPTB Clinical System (Siemens; Malvern, PA, USA). Individual amino acid concentrations were measured following derivatization and separation on an Agilent 1260 liquid chromatograph using Chemstation software. Blood glucose was determined using ACCU-CHEK Compact Plus (Roche Diagnostics; Indianapolis, IN, USA). Plasma glucagon levels were determined using Mercodia glucagon enzyme-linked immunosorbent assay (ELISA) (31).

Western blotting

Liver samples were lysed with ice-cold mitochondria lysis buffer (0.5% Triton, 10 mM Hepes, pH 7.4, 2 mM dithiothreitol) in the presence of protease and phosphatase inhibitor cocktails (Thermo-Fisher; Waltham, MA, USA). Total sample lysates were mixed with 6× sodium dodecyl sulfate (SDS) loading buffer (Alfa-Aesar; Ward Hill, MA, USA) and boiled for 5 minutes. Protein samples (10–20 µg) were loaded and separated on 10%, 12%, or 18% SDS-PAGE gels (Bio-Rad; Hercules, CA, USA) and transferred to polyvinylidene difluoride membranes. The membranes were blocked for 1 hour with 5% bovine serum albumin in 1× tris-buffered saline supplemented with 0.1% Tween20 (Bio-Rad) and incubated with the following antibodies: GS (32), glutaminase 2 (GLS2) (33), OTC (34), and glyceraldehyde-3-phosphate dehydrogenase (35). Bound antibodies were detected using alkaline phosphatase-conjugated anti-goat (36) or horseradish peroxidase-conjugated anti-goat (37), anti-rabbit (38), or anti-mouse (39) secondary antibodies (1:10 000 dilution) and enhanced chemiluminescence reagent (Thermo-Fisher). Band intensities were quantified in ImageQuant TL and Amersham Imager 600 Analysis software.

Ribonucleic acid in situ hybridization

Formalin-fixed pancreatic sections were permeabilized and hybridized with messenger ribonucleic acid (mRNA) probes to GS (*Glul*), *Gls2*, and *Otc* according to the manufacturer's instructions (Advanced Cell Diagnostics; Newark, CA, USA). Following probe hybridization and amplification, *Glul*, *Gls2*, and *Otc* mRNAs were detected using RNAscope 2.5 BROWN staining Kit, and images were obtained using a Zeiss Axio Scan.Z1 slide scanner (Zeiss; Oberkochen, Germany). *Glul*-, *Gls2*-, and *Otc*-positive areas were quantified using the HALO image analysis software (Indica Labs; Albuquerque, NM, USA).

RNA sequencing preparation and analysis

Total RNA was purified using MagMAX-96 for Microarrays Total RNA Isolation Kit (Ambion by Life Technologies; Waltham, MA, USA), according to manufacturer's specifications. Genomic deoxyribonucleic acid was removed using MagMAX Turbo DNase Buffer and TURBO DNase from the MagMAX kit listed above (Ambion by Life Technologies). Strand-specific RNA-seq libraries were prepared using KAPA mRNA-Seq Library Preparation Kit (Kapa Biosystems; Wilmington, MA, USA). Twelve-cycle PCR was performed to amplify libraries. Sequencing was performed on Illumina HiSeq 2000 (Illumina; San Diego, CA, USA) by multiplexed single-read run with 33 cycles. Raw sequence data (binary base call [BCL] files) were converted to FASTQ format via Illumina Casava 1.8.2. Reads were decoded based on their barcodes and read quality was evaluated with FastQC (http://www.bioinformatics.babraham.ac.uk/projects/fastqc/). Reads were mapped to the mouse transcriptome (NCBI GRCm38) using ArrayStudio software (OmicSoft, Cary, North Carolina), allowing 2 mismatches. Reads mapped to the exons of a gene were summed at the gene level. Differential expressed

genes were identified by DESeq2 package and significantly perturbed genes were defined with fold changes no less than 1.5 in either an up or down direction and with $P < 0.01$.

Histology

Pancreata were fixed in 10% neutral buffered formalin solution for 48 hours and then embedded in paraffin. Two sections of the pancreas from each animal were stained with an antiglucagon antibody (40) or an anti-insulin antibody (41), and areas of glucagon and insulin-positive cells were measured using Halo digital imaging analysis software (Indica Labs). The percent of glucagon- and insulin-positive areas in proportion to the whole pancreas area were calculated. The α- and β-cell mass was calculated by multiplying the α- and β-cell area for each animal against their corresponding pancreas weight.

OTC activity

Liver samples were lysed with ice-cold buffer (0.5% Triton, 10 mM Hepes, pH 7.4, 2 mM dithiothreitol). The enzyme activity was measured, as described previously (42). Protein samples (0.5–10 μg) were added to a reaction mixture (5 mM L-ornithine monohydrochloride, 15 mM carbamoyl phosphate dilithium salt, 270 mM triethanolamine, pH 7.7) and incubated at 37°C for 30 minutes. Reactions were stopped by adding a 3:1 phosphoric/sulfuric acid solution. Then, a 3% 2,3-butanedione monoxime was added and the mixture was incubated at 95°C to 100°C for 15 minutes. Citrulline production was determined by measuring absorbance at 490 nm.

Statistics

Statistical analyses were performed utilizing GraphPad software Prism 7.0, with the exception of RNA sequencing data analysis. All parameters were analyzed by student's *t*-test or 1-way or 2-way analysis of variance (ANOVA); a threshold of $P < 0.05$ was considered statistically significant. If a significant F ratio was obtained with ANOVA, post hoc analysis was conducted with Bonferroni post-tests.

Results

Effects of GCGR blocking antibody on plasma ammonia and amino acid levels, body weight, and survival in *Otc*$^{spf\text{-}ash}$ mice

We confirmed previous reports (43, 44) that *Otc*$^{spf\text{-}ash}$ mice on regular chow have a mild phenotype (Table S1 (45)) due to residual OTC activity (Fig. S1; all supplementary material and figures are located in a digital research material repository (45)). To determine the effect of GCGR blocking antibody on the clinical abnormalities of OTC deficiency, we switched *Otc*$^{spf\text{-}ash}$ (n = 20) and wild-type mice (n = 20) from a regular chow diet (21% protein) to a high-protein diet (30% protein; day 0). On day 2, plasma ammonia was measured to confirm elevated levels in *Otc*$^{spf\text{-}ash}$ mice (Fig. 1A). The mice were sorted into 2 groups per genotype based on day 2 plasma ammonia levels. From day 2 to the end of the study, half of the *Otc*$^{spf\text{-}ash}$ (n = 10) and wild-type mice (n = 10) received weekly subcutaneous injections of GCGR antibody at 10 mg/kg, whereas the other mice were dosed weekly with the control antibody at 10 mg/kg. On average, the GCGR antibody lowered plasma ammonia in *Otc*$^{spf\text{-}ash}$ mice (162 umol/L) by half relative to the control antibody (327 umol/L) (Fig. 1A). The control antibody treated *Otc*$^{spf\text{-}ash}$ mice lost 20% of their body weight over the course of the study, whereas wild-type mice gained 30% weight. The GCGR antibody-treated *Otc*$^{spf\text{-}ash}$ mice gained weight amounting to 81% of wild-type mice treated with the GCGR antibody (Fig. 1B). The lower plasma ammonia levels and improved body weights of *Otc*$^{spf\text{-}ash}$ mice treated with the GCGR antibody were associated with higher survival (Fig. 1C). In wild-type mice, the GCGR antibody did not affect plasma ammonia levels, body weight, or survival rate.

Consistent with previous findings (22, 23), we show that GCGR antibody treatment increases circulating amino acid levels (Fig. S2 (45)). Plasma levels of alanine, glutamine and lysine were further elevated in GCGR antibody-treated *Otc*$^{spf\text{-}ash}$ mice, with the highest increase in glutamine (Fig. 1D, Fig. S2; (45)). We and others have previously shown that the elevated plasma amino acid levels promote an increase in pancreas weight, islet number, α-cell mass, and circulating glucagon levels (20, 22, 24). We now extend these observations to *Otc*$^{spf\text{-}ash}$ mice (Fig. S3 (45)). Weight loss in the control antibody administered *Otc*$^{spf\text{-}ash}$ mice was associated with reductions in lean and fat mass (Fig. 2). The GCGR antibody prevented loss of liver and kidney mass, and partially preserved heart and skeletal muscle mass, with minor effects on fat mass. These data show that the GCGR antibody has beneficial effects on plasma ammonia levels, body weight gain, and survival, and is associated with a profound increase in plasma glutamine levels when compared with wild-type mice treated with the antibody.

Gene expression changes in *Otc*$^{spf\text{-}ash}$ mice and effects of the GCGR antibody

RNA sequencing revealed 717 differentially regulated genes in livers from *Otc*$^{spf\text{-}ash}$ mice when compared with

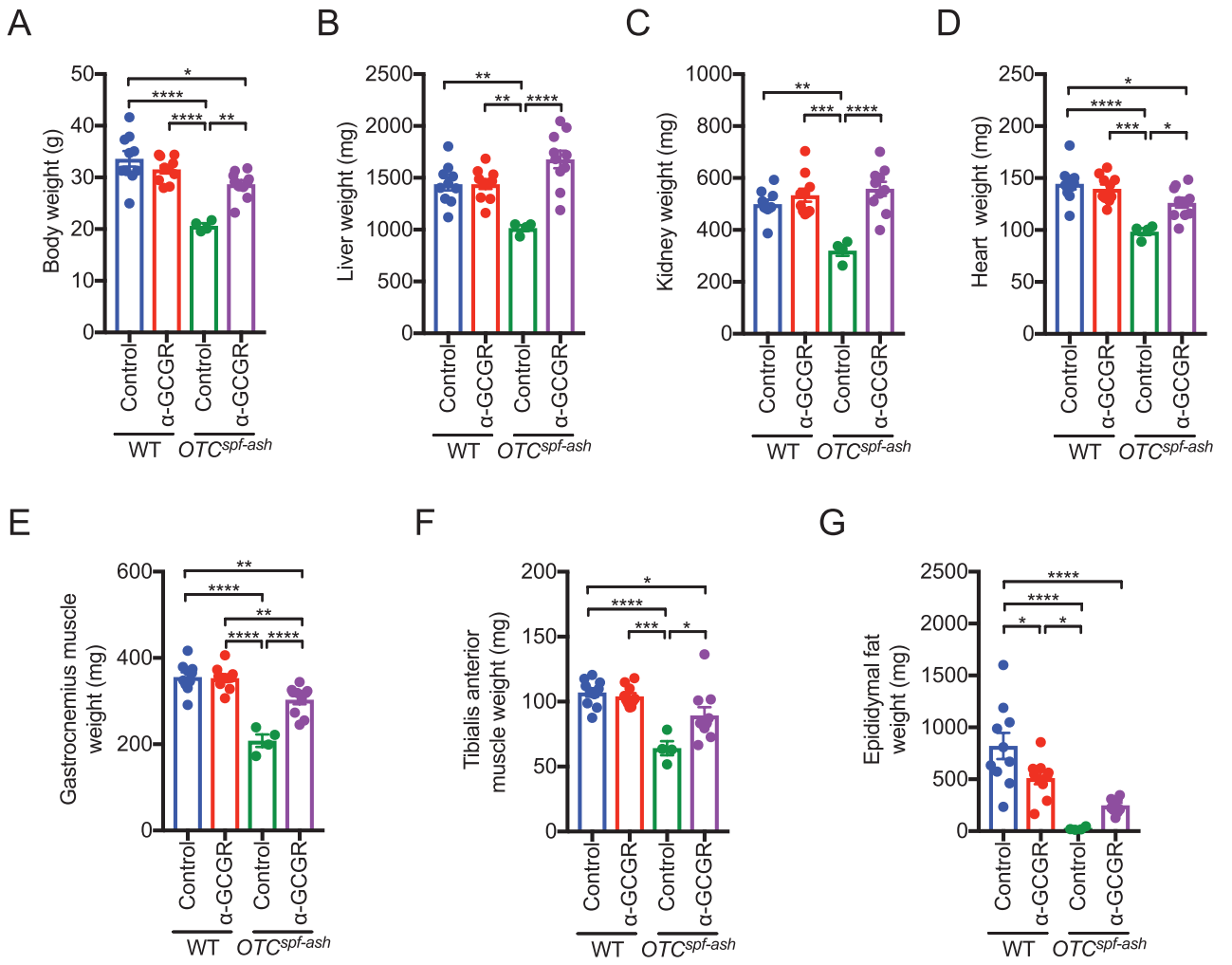

Figure 2. Glucagon receptor (GCGR) inhibition preserves lean organ mass in *Otc*$^{spf\text{-}ash}$ mice on a high-protein diet. Body weights (**A**) in *Otc*$^{spf\text{-}ash}$ and wild-type (WT) mice, placed on a high-protein diet on day 0 and administered with α-GCGR or control antibodies weekly for 54 days from day 2 (10 mg/kg; n = 10 per group at the study inception and n = 4–10 at the study termination due to lethality in *Otc*$^{spf\text{-}ash}$ mice). Liver (**B**), heart (**C**), kidney (**D**), tibialis anterior muscle (**E**), gastrocnemius muscle (**F**), and edidymal fat (**G**) weights for the groups. Data are mean ± standard error of the mean (SEM). Statistical analysis was conducted by 1-way analysis of variance (ANOVA) with Bonferroni post-test. * $P < 0.05$, ** $P < 0.01$, *** $P < 0.001$, **** $P < 0.0001$.

their wild-type counterparts (Fig. 3A and Table S2 (45)). Illumina pathway enrichment analysis identified 6 pathways that are significantly regulated (defined by $P < 1E\text{-}10$) in *Otc*$^{spf\text{-}ash}$ mouse liver. The regulated pathways suggest activation of the innate immune response in *Otc*$^{spf\text{-}ash}$ mice (Fig. 3B), which is in line with altered hepatic immune response previously reported in this model (44). Further analysis showed that 354 genes are differentially regulated by the GCGR antibody in *Otc*$^{spf\text{-}ash}$ mice when compared with *Otc*$^{spf\text{-}ash}$ mice treated with the control antibody (Fig. 3A and Table S2 (45)). A total of 118 genes were common between the 2 groups (Fig. 3A). The heatmap in Fig. 3C shows that 109/118 genes were regulated in opposite directions. Among the 109 genes, glutamic-oxaloacetate transaminase 1 (*Got1*) and *Glul* are involved in amino acid metabolism and ammonia production (Fig. 3D and 3E). Importantly, the expression of *Glul* is restored, whereas *Gls2* expression is reduced by GCGR antibody treatment in *Otc*$^{spf\text{-}ash}$ mice (Fig. 3E and 3F). As expected, *Otc* expression was minimal in *Otc*$^{spf\text{-}ash}$ mice and not affected by the GCGR antibody (Fig. 3G). These data show that the GCGR antibody induces gene expression changes in *Otc*$^{spf\text{-}ash}$ mice favoring hepatic glutamine synthesis and reduced ammonia production.

Liver GLS2, GS, and OTC expression

RNA in situ hybridization confirmed restricted expression of *Glul* to 1 to 2 cell layers around the central vein. Consistent with the gene expression data, *Glul*

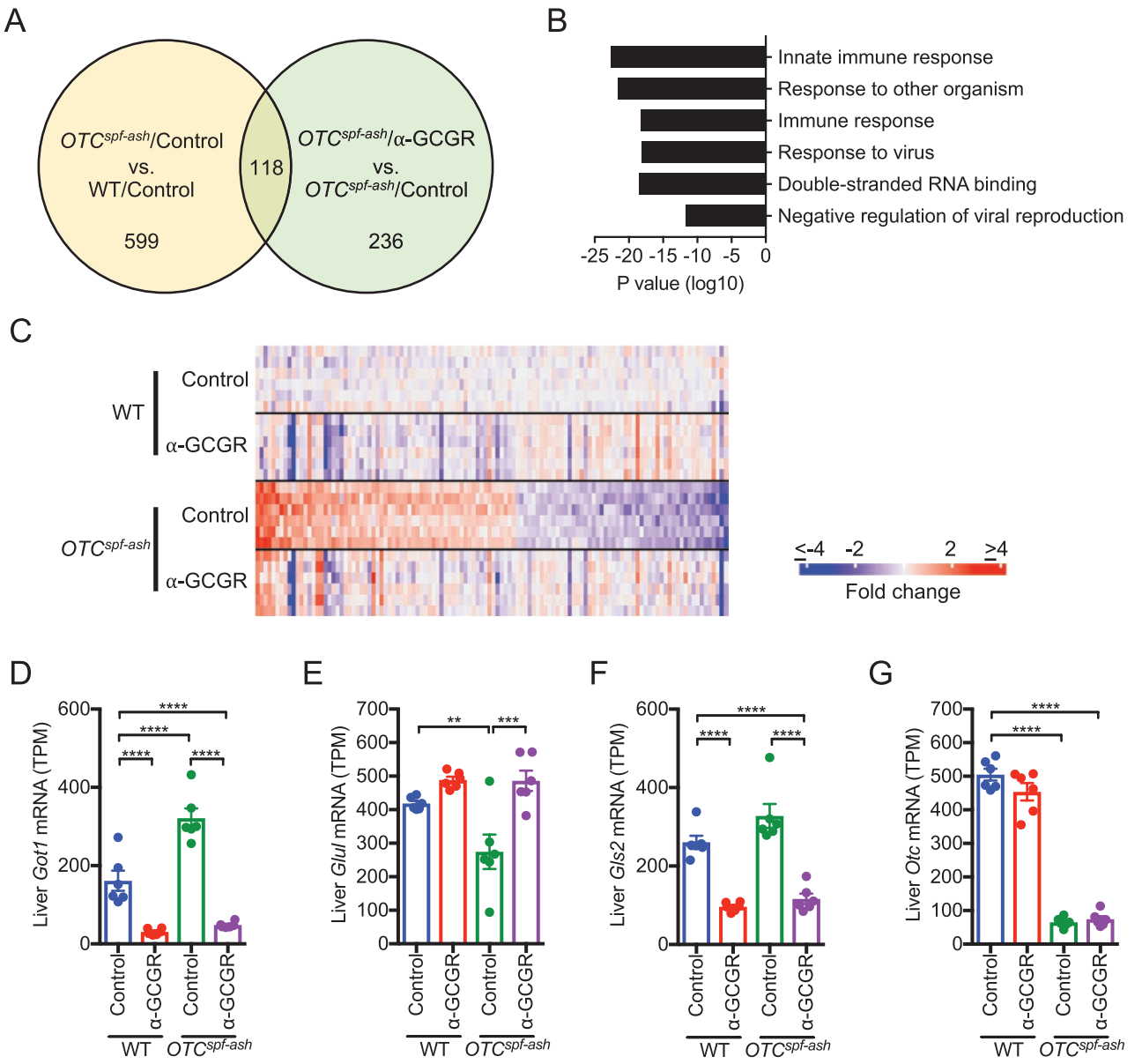

Figure 3. Liver ribonucleic acid (RNA) sequencing demonstrates glucagon receptor (GCGR) antibody-regulated expression of key genes involved in glutamine/glutamate/ammonia metabolism. *Otc*$^{spf\text{-}ash}$ and wild-type (WT) mice placed on a high-protein diet on day 0 and administered weekly with α-GCGR or control antibodies for 39 days from day 2 (10 mg/kg; n = 6 per group). Venn diagram of genes perturbed in *Otc*$^{spf\text{-}ash}$ mice (yellow circle) or regulated by α-GCGR in *Otc*$^{spf\text{-}ash}$ mice (**A**, green circle). Significantly regulated pathways (defined by $P < 1E\text{-}10$) identified by Illumina pathway enrichment analysis of genes perturbed (717 significantly perturbed genes, using DESeq2package defined by fold change ≥ 1.5 in either direction with $P \leq 0.01$) in *Otc*$^{spf\text{-}ash}$ mice (**B**). Four-group heat map of the 118 overlapped genes (**C**) described in the Venn diagram described in (**A**). Transcripts per million (TPM) of each gene for WT/α-GCGR, *Otc*$^{spf\text{-}ash}$/control group, or *Otc*$^{spf\text{-}ash}$/α-GCGR groups was normalized against the mean of the WT/control group, followed by log2 transformation. Genes are organized by fold-change order in the *Otc*$^{spf\text{-}ash}$/α-GCGR group versus the WT/control group. Expression levels (TPM) of *Got1* (**D**), *Glul* (**E**), *Gls2* (**F**), and *Otc* (**G**) in the 4 groups. Statistical analysis was conducted by DESeq2 package, comparing between the 2 WT groups, the 2 *Otc*$^{spf\text{-}ash}$ groups, and the 2 α-GCGR administered groups. Data are mean ± standard error of the mean (SEM). ** $P < 0.01$, *** $P < 0.001$, **** $P < 0.0001$.

expression was reduced in *Otc*$^{spf\text{-}ash}$ mice and restored in GCGR antibody-treated mice (Fig. 4A and 4B). The expression of *Gls2* is widespread (periportal hepatocytes) in *Otc*$^{spf\text{-}ash}$ and wild-type mice and reduced by the GCGR antibody (Fig. 4C and 4D). *Otc* expression is detected in all hepatocytes and is minimal in *Otc*$^{spf\text{-}ash}$ mice (Fig. 4E and 4F). The data were confirmed by western blotting of livers from *Otc*$^{spf\text{-}ash}$ and wild-type mice treated with GCGR or control antibodies (Fig. 5A–5F). Note the strong reduction in GS and full restoration of expression in *Otc*$^{spf\text{-}ash}$ mice by the GCGR antibody (Fig. 5A and 5B).

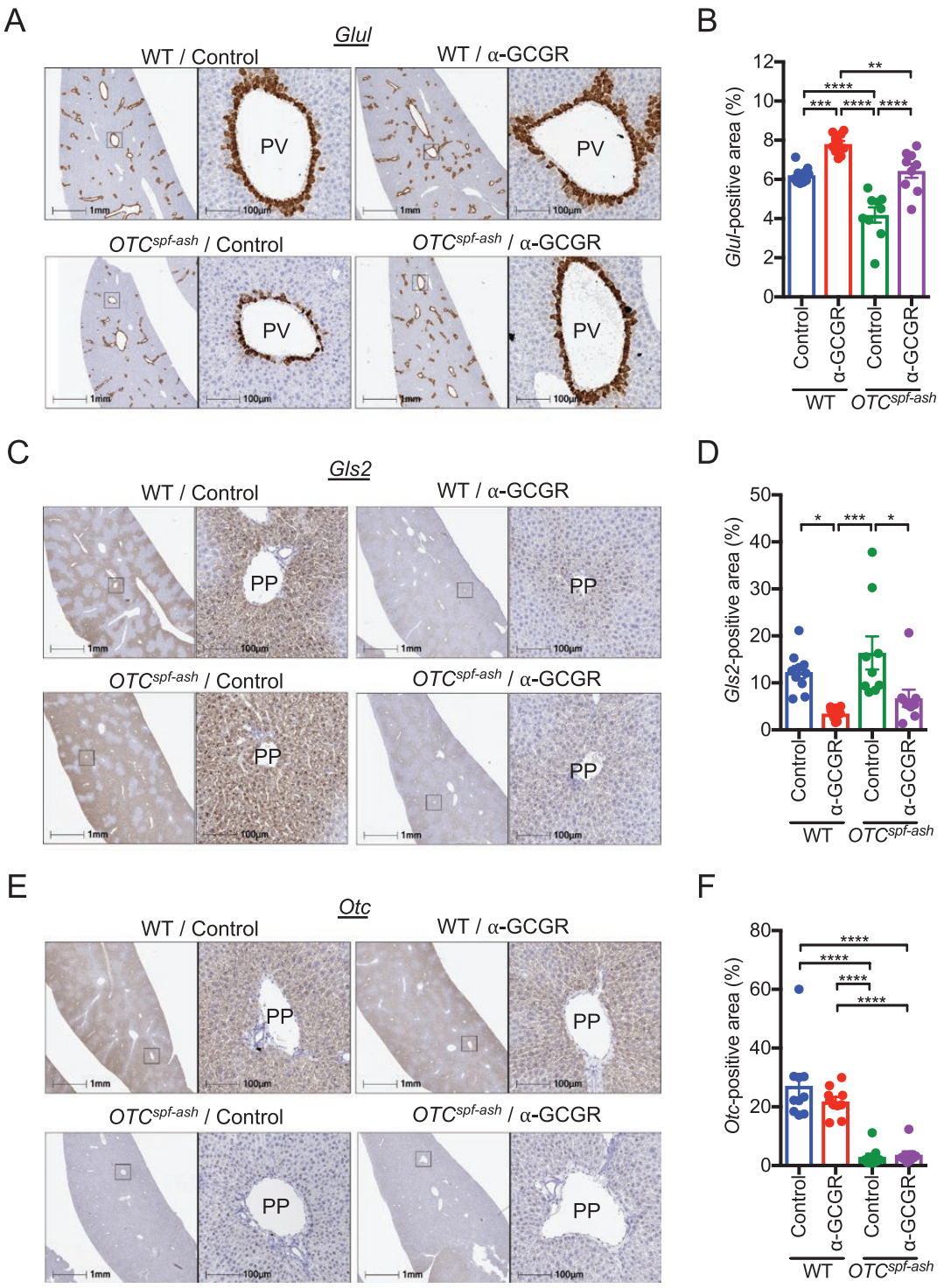

Figure 4. Opposing effects of ornithine transcarbamylase (OTC) inactivation and glucagon receptor (GCGR) blockade on messenger RNA (mRNA) expressions of the key glutamine/glutamate metabolism genes, *Glul* and *Gls2*. Liver RNA fluorescent in situ hybridization (RNA-FISH) images of *Glul* (**A**), *Gls2* (**C**), or *Otc* (**E**) and respective quantifications of RNA-ISH-positive areas (**B**, **D**, **F**) in the 4 groups (n = 9–10 per group), as described in Fig. 2. Data are mean ± standard error of the mean (SEM). Statistical analysis was conducted by 1-way analysis of variance (ANOVA) with Bonferroni post-test (**B**, **D**, **F**). * $P < 0.05$, ** $P < 0.01$, *** $P < 0.001$, **** $P < 0.0001$.

Discussion

The key finding is that a GCGR-blocking antibody reduced hyperammonemia and lethality of $Otc^{spf\text{-}ash}$ mice on a high-protein diet. The reduction in plasma ammonia was accompanied by increased plasma glutamine levels and reduced hepatic expression of glutaminase, which catabolizes

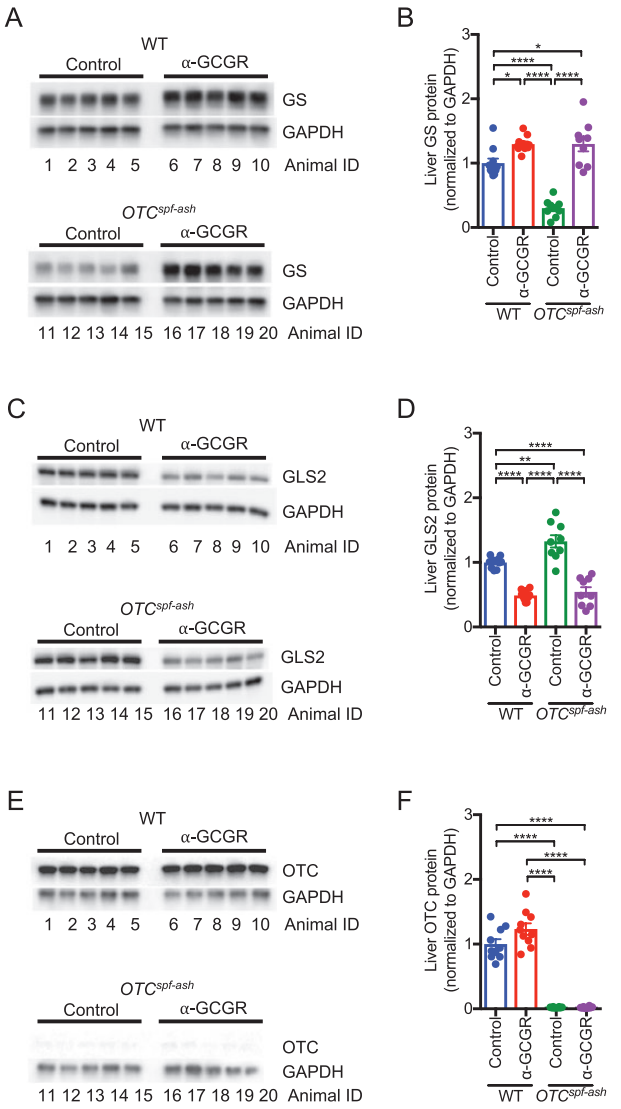

Figure 5. Opposing effects of ornithine transcarbamylase (OTC) inactivation and glucagon receptor (GCGR) blockade on protein levels of the key glutamine/glutamate metabolism proteins, glutamine synthetase (GS) and glutaminase 2 (GLS2). Liver western blotting images of GS (**A**), GLS2 (**C**), or OTC (**E**) and respective quantifications of blotting bands (**B**, **D**, **F**) in the 4 groups (n = 9–10 per group), as described in Fig. 2. Data are mean ± standard error of the mean (SEM). Statistical analysis was conducted by 1-way analysis of variance (ANOVA) with Bonferroni post-test (**B**, **D**, **F**). * $P < 0.05$, ** $P < 0.01$, **** $P < 0.0001$.

glutamine to glutamate and ammonia, and increased expression of GS, which carries out the opposite reaction. The GCGR antibody-treated *Otc*$^{spf\text{-}ash}$ mice gained weight close to their wild-type counterparts, with preservation of lean mass.

Glucagon promotes hepatic amino acid uptake and metabolism, including utilization of amino acids for gluconeogenesis. Consistent with this role of glucagon, we observed increased plasma amino acid levels, in particular glutamine, and lower blood glucose in *Otc*$^{spf\text{-}ash}$ and wild-type mice treated with the GCGR antibody. We speculate that decreased glutamine catabolism was a major driver of lower blood glucose levels in *Otc*$^{spf\text{-}ash}$ and wild-type mice treated with the GCGR antibody. The higher plasma levels of glutamine in *Otc*$^{spf\text{-}ash}$ mice relative to treated wild-type mice is likely secondary to minimal urea cycle activity.

Feeding *Otc*$^{spf\text{-}ash}$ mice a high-protein diet induced progressive weight loss due to reductions in both lean and fat mass. The GCGR antibody prevented lean mass loss with little impact on fat mass. As amino acids stimulate cell growth via activation of the mTOR pathway, we speculate that increased plasma amino acids in GCGR antibody-treated *Otc*$^{spf\text{-}ash}$ mice provide the substrates or signal necessary for the lean organs to maintain their mass. The GCGR antibody fully restored liver and kidney mass, whereas the effect was partial in heart and skeletal muscle. This may reflect differences in the organs' ability to sense or utilize elevated levels of amino acids for cell growth. Furthermore, ammonia uptake by the skeletal muscle and conversion to glutamine could affect the pool of amino acids required for protein synthesis (46–48). Continuous ammonia detoxification in muscle could also lead to autophagy and mitochondrial dysfunction (49, 50). In kidneys, elevated ammonia levels might impair renal function through glomerular injury and tubulointestinal fibrosis (51). We speculate that the ability of the GGGR antibody to preserve lean mass is important for survival of *Otc*$^{spf\text{-}ash}$ mice. The GCGR antibody did not increase lean organ mass in wild-type mice, indicating GCGR inhibition-induced cell growth develops only when compromised with the notable exception of the pancreas which is an integral part of the liver—pancreas axis (see below for discussion). The fat mass was reduced in high-protein diet fed wild-type mice administered with the GCGR antibody compared with the counterparts administered with the control antibody. A potential explanation is an increased utilization of adipose tissues for energy in the GCGR antibody-treated animals due to reduced amino acid catabolism, followed by insufficient extraction of energy from a protein-rich diet (30% by weight or 35% by kcal). The GCGR antibody treatment in high-protein diet fed wild-type mice led to a reduction in OTC activity without changes in OTC mRNA or protein levels, indicating post-translational regulation of OTC activity. This may be a result of increased hepatic amino acid concentrations inhibiting OTC catalytic activity via acetylation of a lysine residue involved in substrate binding and catalysis (52, 53).

We and others have reported GCGR inhibition-induced hyperaminoacidemia accompanies reduced hepatic expression of amino acid transporter and catabolism genes, including *Gls2* in chow-fed wild-type mice (20, 22, 26). Similarly, we found that GCGR inhibition reduced *Gls2* expression in wild-type and OTC$^{spf\text{-}ash}$ mice on a high-protein

diet. A gene expression change observed in this study, but not in previous studies, was the increased hepatic *Glul* expression in OTC$^{spf\text{-}ash}$ mice. This may be a consequence of GCGR inhibition in the hyperammonemic setting, as the GCGR antibody did not change *Glul* expressions in wild-type mice on a high-protein diet (ie, this study) or a regular chow diet (22). Elucidation of the signaling cascade of *Gls2* and *Glul* transcriptional regulation following GCGR inhibition is beyond the scope of this study, but could involve the cAMP responsible binding element (CREB) protein, a master GCGR signaling mediator, which controls the transcription of genes involved in glucose, amino acid, and lipid metabolism in the liver (54). Another potential mediator is CREB-regulated transcription coactivator 2 (CRTC2), which plays a key role in glucagon-induced expression of several hepatic amino acid catabolism genes, including *Got1* and *Gpt1* (55).

Ammonia is produced in all organs but can only be detoxified to urea in the liver. In other organs, ammonia is temporarily detoxified by incorporation into glutamine, which is released into plasma to be safely transported between organs to maintain nitrogen balance. Glutamine is taken up by the liver and catabolized to ammonia for further processing. The zonation of the liver provides for efficient control of ammonia levels. Urea synthesis takes place in the periportal hepatocytes, whereas the hepatocytes close to the central vein are specialized in the synthesis of glutamine. The latter is a very efficient process since 5% to 10% of the hepatocyte pool removes one-third of the total ammonia in the liver (11, 56–59). This implies that increasing the expression and number of GS-positive hepatocytes could be an important mechanism for the regulation of plasma ammonia levels. We speculate that a GCGR inhibition-induced increase in the *Glul*-positive area and GS expression could be a major contributor to the control of hyperammonemia in *Otc*$^{spf\text{-}ash}$ mice. The other key mechanism for the control of plasma ammonia levels is the reduced expression of glutaminase in the periportal hepatocytes. In summary, our data indicate that GCGR inhibition ameliorates hyperammonemia, in part by promoting the incorporation of nitrogen into glutamine. Improved hyperammonemia in combination with the preservation of lean organ mass increased survival of *Otc*$^{spf\text{-}ash}$ mice treated with GCGR blocking antibody.

Recent research shows the existence of a liver–pancreatic–α-cell axis where glucagon is the messenger from the α-cells to the liver and glutamine is the mediator from the liver to the α-cells (20, 22, 60, 61). Disruption of the liver–α-cell axis results in elevated plasma levels of glucagon and glutamine as well as α-cell hyperplasia and increased pancreas weight (21, 22). We extend these observations to *Otc*$^{spf\text{-}ash}$ mice. Interestingly, the changes in plasma glucagon levels and α-cell hyperplasia were the same between *Otc*$^{spf\text{-}ash}$ and wild-type mice despite higher circulating levels of glutamine in *Otc*$^{spf\text{-}ash}$ mice. This suggests that maximal rates of α-cell hyperplasia and glucagon secretion are reached in the treated wild-type mice. α-cell hyperplasia is a potential safety concern, which needs to be considered when using the GCGR antibody. Pancreas weight was reduced in *Otc*$^{spf\text{-}ash}$ mice and was overcorrected by the GCGR antibody treatment, indicating the possibility that GCGR inhibition prevents functional decline in the pancreas of *Otc*$^{spf\text{-}ash}$ mice.

In conclusion, we show that GCGR inhibition using a monoclonal antibody could reduce risk for hyperammonemia and other clinical manifestations of patients with defects in the urea cycle or suffering from liver injury or failure and GS deficiency.

Acknowledgments

We would like to thank Jinny Johnson at Protein Chemistry Lab, Texas A&M University for help with the amino acid quantification and Angelos Papatheodorou with the plasma ammonia assay.

Financial support: The studies were funded by Regeneron Pharmaceuticals.

Author Contributions: K.C., B.S., and E.N. conducted experiments and analyzed data. Q.S., J.K., and X.C. analyzed data. K.C., J.G., and H.O. designed experiments and wrote the manuscript.

Additional Information

Correspondence:Haruka Okamoto, PhD, Regeneron Pharmaceuticals Inc, 777 Old Saw Mill River Rd, Tarrytown, New York 10591, USA. E-mail: haruka.okamoto@regeneron.com.

Disclosure Summary: All authors are or were employees and shareholders of Regeneron Pharmaceuticals.

Data Availability: Data generated or analyzed during this study are included in this published article or in the data repositories listed in References.

References

1. Cruzat V, Macedo Rogero M, Noel Keane K, Curi R, Newsholme P. Glutamine: metabolism and immune function, supplementation and clinical translation. *Nutrients*. 2018;**10**(11):1564.
2. Gallagher RC, Lam C, Wong D, Cederbaum S, Sokol RJ. Significant hepatic involvement in patients with ornithine transcarbamylase deficiency. *J Pediatr.* 2014;**164**(4): 720–725.e6.
3. Gropman AL, Summar M, Leonard JV. Neurological implications of urea cycle disorders. *J Inherit Metab Dis*. 2007;**30**(6):865–879.
4. Scaglia F, Brunetti-Pierri N, Kleppe S, et al. Clinical consequences of urea cycle enzyme deficiencies and potential links to arginine and nitric oxide metabolism. *J Nutr.* 2004;**134**(10 Suppl):2775S–2782S; discussion 2796S.

5. Yaplito-Lee J, Chow CW, Boneh A. Histopathological findings in livers of patients with urea cycle disorders. *Mol Genet Metab*. 2013;**108**(3):161–165.
6. Hakvoort TB, He Y, Kulik W, et al. Pivotal role of glutamine synthetase in ammonia detoxification. *Hepatology*. 2017;**65**(1):281–293.
7. Häussinger D, Schliess F. Glutamine metabolism and signaling in the liver. *Front Biosci*. 2007;**12**:371–391.
8. Watford M. Glutamine and glutamate metabolism across the liver sinusoid. *J Nutr*. 2000;**130**(4S Suppl):983S–987S.
9. Clay AS, Hainline BE. Hyperammonemia in the ICU. *Chest*. 2007;**132**(4):1368–1378.
10. Smith W, Kishnani PS, Lee B, et al. Urea cycle disorders: clinical presentation outside the newborn period. *Crit Care Clin*. 2005;**21**(4 Suppl):S9–17.
11. Walker V. Ammonia metabolism and hyperammonemic disorders. *Adv Clin Chem*. 2014;**67**:73–150.
12. Brassier A, Gobin S, Arnoux JB, et al. Long-term outcomes in Ornithine Transcarbamylase deficiency: a series of 90 patients. *Orphanet J Rare Dis*. 2015;**10**:58.
13. Campbell AG, Rosenberg LE, Snodgrass PJ, Nuzum CT. Ornithine transcarbamylase deficiency: a cause of lethal neonatal hyperammonemia in males. *N Engl J Med*. 1973;**288**(1):1–6.
14. Unsinn C, Das A, Valayannopoulos V, et al. Clinical course of 63 patients with neonatal onset urea cycle disorders in the years 2001-2013. *Orphanet J Rare Dis*. 2016;**11**(1):116.
15. Auron A, Brophy PD. Hyperammonemia in review: pathophysiology, diagnosis, and treatment. *Pediatr Nephrol*. 2012;**27**(2):207–222.
16. Häberle J, Boddaert N, Burlina A, et al. Suggested guidelines for the diagnosis and management of urea cycle disorders. *Orphanet J Rare Dis*. 2012;**7**:32.
17. Longo N, Holt RJ. Glycerol phenylbutyrate for the maintenance treatment of patients with deficiencies in enzymes of the urea cycle. *Expert Opin Orphan Drugs*. 2017;**5**(2):999–1010.
18. Boden G, Master RW, Rezvani I, Palmer JP, Lobe TE, Owen OE. Glucagon deficiency and hyperaminoacidemia after total pancreatectomy. *J Clin Invest*. 1980;**65**(3):706–716.
19. Muller WA, Berger M, Suter P, et al. Glucagon immunoreactivities and amino acid profile in plasma of duodenopancreatectomized patients. *J Clin Invest*. 1979;**63**(5):820–827.
20. Dean ED, Li M, Prasad N, et al. Interrupted glucagon signaling reveals hepatic α cell axis and role for L-glutamine in α cell proliferation. *Cell Metab*. 2017;**25**(6):1362–1373.e5.
21. Galsgaard KD, Winther-Sørensen M, Ørskov C, et al. Disruption of glucagon receptor signaling causes hyperaminoacidemia exposing a possible liver-alpha-cell axis. *Am J Physiol Endocrinol Metab*. 2018;**314**(1):E93–E103.
22. Kim J, Okamoto H, Huang Z, et al. Amino acid transporter Slc38a5 controls glucagon receptor inhibition-induced pancreatic α cell hyperplasia in mice. *Cell Metab*. 2017;**25**(6):1348–1361.e8.
23. Okamoto H, Kim J, Aglione J, et al. Glucagon receptor blockade with a human antibody normalizes blood glucose in diabetic mice and monkeys. *Endocrinology*. 2015;**156**(8):2781–2794.
24. Solloway MJ, Madjidi A, Gu C, et al. Glucagon couples hepatic amino acid catabolism to mTOR-dependent regulation of α-cell mass. *Cell Rep*. 2015;**12**(3):495–510.
25. Watanabe C, Seino Y, Miyahira H, et al. Remodeling of hepatic metabolism and hyperaminoacidemia in mice deficient in proglucagon-derived peptides. *Diabetes*. 2012;**61**(1):74–84.
26. Cheng X, Kim SY, Okamoto H, et al. Glucagon contributes to liver zonation. *Proc Natl Acad Sci U S A*. 2018;**115**(17):E4111–E4119.
27. Rivera-Barahona A, Sánchez-Alcudia R, Viecelli HM, et al. Functional characterization of the spf/ash splicing variation in OTC deficiency of mice and man. *Plos One*. 2015;**10**(4):e0122966.
28. Yang Y, Wang L, Bell P, et al. A dual AAV system enables the Cas9-mediated correction of a metabolic liver disease in newborn mice. *Nat Biotechnol*. 2016;**34**(3):334–338.
29. *RRID:AB_2783540*.
30. *RRID:AB_2783872*.
31. *RRID:AB_2783839*.
32. *RRID:AB_397880*.
33. *RRID:AB_11031431*.
34. *RRID:AB_2876368*.
35. *RRID:AB_561053*.
36. *RRID:AB_2340393*.
37. *RRID:AB_2340390*.
38. *RRID:AB_2307391*.
39. *RRID:AB_10015289*.
40. *RRID:AB_2783539*.
41. *RRID:AB_2617169*.
42. Ye X, Robinson MB, Batshaw ML, Furth EE, Smith I, Wilson JM. Prolonged metabolic correction in adult ornithine transcarbamylase-deficient mice with adenoviral vectors. *J Biol Chem*. 1996;**271**(7):3639–3646.
43. Doolittle DP, Hulbert LL, Cordy C. A new allele of the sparse fur gene in the mouse. *J Hered*. 1974;**65**(3):194–195.
44. McGuire PJ, Tarasenko TN, Wang T, et al. Acute metabolic decompensation due to influenza in a mouse model of ornithine transcarbamylase deficiency. *Dis Model Mech*. 2014;**7**(2):205–213.
45. Cavino K, Sung B, Su Q, et al. Data from: data from: glucagon receptor inhibition reduces hyperammonemia and associated lethality in a mouse model of urea cycle disorder. Figshare 2020. Deposited October 12, 2020. Doi:10.6084/m9.figshare.13082249.
46. Dam G, Ott P, Aagaard NK, Vilstrup H. Branched-chain amino acids and muscle ammonia detoxification in cirrhosis. *Metab Brain Dis*. 2013;**28**(2):217–220.
47. Jindal A, Jagdish RK. Sarcopenia: ammonia metabolism and hepatic encephalopathy. *Clin Mol Hepatol*. 2019;**25**(3):270–279.
48. Qiu J, Thapaliya S, Runkana A, et al. Hyperammonemia in cirrhosis induces transcriptional regulation of myostatin by an NF-κB-mediated mechanism. *Proc Natl Acad Sci U S A*. 2013;**110**(45):18162–18167.
49. Qiu J, Tsien C, Thapalaya S, et al. Hyperammonemia-mediated autophagy in skeletal muscle contributes to sarcopenia of cirrhosis. *Am J Physiol Endocrinol Metab*. 2012;**303**(8):E983–E993.
50. Davuluri G, Allawy A, Thapaliya S, et al. Hyperammonaemia-induced skeletal muscle mitochondrial dysfunction results in cataplerosis and oxidative stress. *J Physiol*. 2016;**594**(24):7341–7360.

51. Ling H, Ardjomand P, Samvakas S, et al. Mesangial cell hypertrophy induced by NH4Cl: role of depressed activities of cathepsins due to elevated lysosomal pH. *Kidney Int*. 1998;**53**(6):1706–1712.
52. Zhao S, Xu W, Jiang W, et al. Regulation of cellular metabolism by protein lysine acetylation. *Science*. 2010;**327**(5968):1000–1004.
53. Yu W, Lin Y, Yao J, et al. Lysine 88 acetylation negatively regulates ornithine carbamoyltransferase activity in response to nutrient signals. *J Biol Chem*. 2009;**284**(20):13669–13675.
54. Janah L, Kjeldsen S, Galsgaard KD, et al. Glucagon receptor signaling and glucagon resistance. *Int J Mol Sci*. 2019;**20**(13):3314.
55. Erion DM, Kotas ME, McGlashon J, et al. cAMP-responsive element-binding protein (CREB)-regulated transcription coactivator 2 (CRTC2) promotes glucagon clearance and hepatic amino acid catabolism to regulate glucose homeostasis. *J Biol Chem*. 2013;**288**(22):16167–16176.
56. Brosnan ME, Brosnan JT. Hepatic glutamate metabolism: a tale of 2 hepatocytes. *Am J Clin Nutr.* 2009;**90**(3):857S–861S.
57. Häussinger D. Regulation of hepatic ammonia metabolism: the intercellular glutamine cycle. *Adv Enzyme Regul*. 1986;**25**:159–180.
58. Häussinger D, Lamers WH, Moorman AF. Hepatocyte heterogeneity in the metabolism of amino acids and ammonia. *Enzyme*. 1992;**46**(1-3):72–93.
59. Kari FW, Yoshihara H, Thurman RG. Urea synthesis from ammonia in periportal and pericentral regions of the liver lobule. Effect of oxygen. *Eur J Biochem*. 1987; **163**(1):1–7.
60. Wewer Albrechtsen NJ, Færch K, Jensen TM, et al. Evidence of a liver-alpha cell axis in humans: hepatic insulin resistance attenuates relationship between fasting plasma glucagon and glucagonotropic amino acids. *Diabetologia*. 2018;**61**(3):671–680.
61. Wewer Albrechtsen NJ, Junker AE, Christensen M, et al. Hyperglucagonemia correlates with plasma levels of non-branched-chain amino acids in patients with liver disease independent of type 2 diabetes. *Am J Physiol Gastrointest Liver Physiol*. 2018;**314**(1):G91–G96.